Modulation of magnon spin transport in a magnetic gate transistor

K. S. Das [1,*] F. Feringa,[1] M. Middelkamp,[1] B. J. van Wees,[1,†] and I. J. Vera-Marun [2,‡]

[1]*Physics of Nanodevices, Zernike Institute for Advanced Materials, University of Groningen, 9747 AG Groningen, The Netherlands*

[2]*School of Physics and Astronomy, University of Manchester, Manchester M13 9PL, United Kingdom*

(Received 30 August 2019; revised manuscript received 30 January 2020; accepted 30 January 2020; published 25 February 2020)

We demonstrate a modulation of up to 18% in the magnon spin transport in a magnetic insulator ($Y_3Fe_5O_{12}$, YIG) using a common ferromagnetic metal (permalloy, Py) as a magnetic control gate. A Py electrode, placed between two Pt injector and detector electrodes, acts as a magnetic gate in our prototypical magnon transistor device. By manipulating the magnetization direction of Py with respect to that of YIG, the transmission of magnons through the Py | YIG interface can be controlled, resulting in a modulation of the nonequilibrium magnon density in the YIG channel between the Pt injector and detector electrodes. This study opens up the possibility of using the magnetic gating effect for magnon-based spin logic applications.

DOI: 10.1103/PhysRevB.101.054436

I. INTRODUCTION

Magnon-based spintronic devices are alternatives for charge-based electronics [1–3]. Information, in the form of spin waves or magnons, can be transmitted over a long distance in magnetic insulators [4], without the necessity of accompanying electron transport. Thus magnon-based devices can be used as a new type of interconnects in spintronic circuitry. Additionally, the modulation of magnon spin transport would also enable the use of such devices for logic operations [5]. This has led to a recent surge in experiments exploring the control of magnon transport via magnon-valves [6–8] and in the magnon transistor geometry [9].

In order to implement magnonic logic devices, two distinctive features are important: control of the magnon spin transport and storage of information in a memory device. The presence of both functionalities in a single device is still missing in the previous mentioned magnon valves and magnon transistor. In this work we present a solution using a different principle of operation for a magnon transistor, making use of a magnetic gating effect. Such a transistor operates in the absence of any electrical bias in the control gate, via the modulation of magnon absorption at the YIG | gate interface. This principle of operation, unexplored in previous magnon transistors [9], has the potential to implement nonvolatile memory and enable low-power programmable magnonics.

The ferromagnetic metal permalloy (Py) is used in a proof-of-concept device geometry for demonstrating the modulation of magnon spin transport in a magnetic insulator (YIG) via the magnetic gating effect. Exchange (thermal) magnons are injected using a Pt electrode via the spin Hall effect (SHE), resulting in a nonequilibrium magnon accumulation in the YIG film [4,10]. A second Pt electrode is used to electrically detect the nonequilibrium magnons via the inverse spin Hall effect (ISHE). A middle Py strip is placed between the Pt injector and detector electrodes for manipulating the magnon transport in the YIG channel via the magnetic gating effect, schematically depicted in Fig. 1(a). When a magnon arrives at the YIG | Py interface, three magnon absorption mechanisms are possible: spin-flip scattering at the interface generating a spin accumulation in the Py, spin transfer torque, and magnon to magnon transmission across the YIG | Py interface. The spin transfer torque is maximum when the Py and the YIG magnetizations, M_{Py} and M_{YIG}, are oriented perpendicular to each other. When M_{Py} and M_{YIG} are oriented parallel to each other, the transmission of magnons from the YIG film into the Py strip and spin-flip scattering at the interface is maximized. Considering a shorter magnon mean free path in Py as compared to YIG [11,12], the transmission of magnons into the Py would lead to a decrease in the nonequilibrium magnon density in the YIG channel. This will result in the modulation of the nonlocal magnon spin signal measured by the Pt detector as a function of the relative orientation between M_{Py} and M_{YIG}. Therefore, if spin transfer torque is a dominant process, a decrease of the magnon current is expected when M_{Py} and M_{YIG} are oriented perpendicular. When spin-flip scattering and magnon to magnon transmission are dominant a decrease of the magnon current is expected for parallel alignment of M_{Py} and M_{YIG}. The similar geometry as in Ref. [9] has been used, but the modulation mechanism is completely different in nature. The modulation in Ref. [9] is achieved by creating a nonequilibrium magnon density in the YIG via the electrically driven Pt modulator, whereas in this work the magnons in the YIG channel are in equilibrium with the modulator. We demonstrate that a modulation of up to 18% can be achieved in our devices, which is more than an order of magnitude higher than that reported in Ref. [9] for the same YIG film thickness (210 nm), using a Pt modulator.

*k.s.das@rug.nl

†b.j.van.Wees@rug.nl

‡ivan.veramarun@manchester.ac.uk

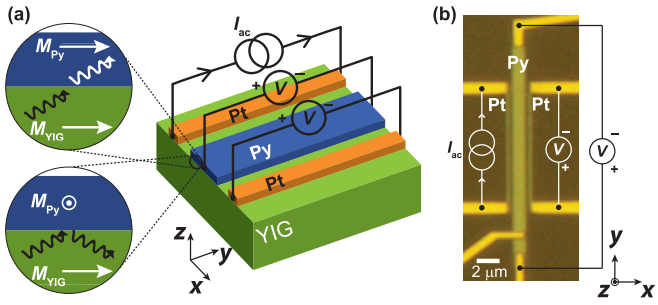

FIG. 1. (a) Schematic illustration of the device geometry. The magnon-valve effect is depicted in the insets, where the transmission of magnons across the Py | YIG interface is dependent on the relative orientation of the Py (M_{Py}) and the YIG (M_{YIG}) magnetizations. (b) An optical image of the device is shown, along with the electrical connections for the nonlocal magnon transport experiment. The center-to-center distance between the Pt injector and the Pt detector is 2 μm for all the devices.

II. EXPERIMENTAL DETAILS

Three batches of devices were fabricated using electron beam lithography on 210 nm thick YIG (111) films, grown by liquid-phase epitaxy on GGG ($Gd_3Ga_5O_{12}$) substrates. 7 nm thick Pt strips, with widths of 200 nm, were dc sputtered on YIG as the injector and detector electrodes. The dimensions of the middle Py strip, also fabricated by dc sputtering, were varied among the different batches of devices. In the first two batches we varied the Py width (300, 500, 600, and 900 nm), while keeping a constant thickness of 9 nm, whereas in the third batch we varied the Py thickness (9, 15, and 38 nm), while keeping a constant width of 900 nm. A Pt-Pt device without any middle Py strip was fabricated as a reference device. The center-to-center distance between the Pt injector and detector electrodes was kept constant at 2 μm for all the devices. An optical image of a device with a 900 nm wide middle Py strip is shown in Fig. 1(b), along with the electrical connections. An alternating current (I), with an rms amplitude of 400 μA and frequency of 11 Hz, was sourced through the Pt injector (left). The first ($1f$) and the second harmonic ($2f$) responses of the nonlocal voltage (V) correspond to the electrically injected (via the SHE) and the thermally injected (via the spin Seebeck effect driven by Joule heating at the injector) magnons. Both responses were measured simultaneously across the Pt detector and the middle Py strip by a phase-sensitive lock-in detection technique. The nonlocal magnon spin signal is defined as $R_{NL}^{1f} = V^{1f}/I$ for the electrically injected magnons, and $R_{NL}^{2f} = V^{2f}/I^2$ for the thermally injected magnons. All the measurements were carried out at room temperature.

III. RESULTS AND DISCUSSION

An external magnetic field (B) was swept along the hard axis (x-axis) direction of the magnetic gate and the corresponding R_{NL}^{1f} measured, as shown in Figs. 2(a)–2(c). A modulation in R_{NL}^{1f}, measured by the Pt detector in the devices with a middle Py, was observed [see Fig. 2(a)]. The maximum value of R_{NL}^{1f} occurs at $B = 0$, when M_{Py} is oriented along the easy axis of the magnetic gate (y axis), perpendicular to M_{YIG}. Note that due to a low coercive field of our YIG film (<1 mT) [13], M_{YIG} is essentially always oriented along the x axis in our measurements. Besides, any possible interfacial exchange interaction between Py and YIG doesn't play a significant role [14,15] and therefore M_{YIG} and M_{Py} can move freely with respect to each other. By changing the magnitude of B, R_{NL}^{1f} was modulated, reaching a minimum value at $|B| \approx 50$ mT, corresponding to the tilting of M_{Py} along the in-plane hard axis direction (x axis) of the magnetic gate. For $|B| \geqslant 50$ mT, when M_{Py} and M_{YIG} are aligned parallel to each other, R_{NL}^{1f} decreases to its minimum value, corresponding to a modulation (ΔR^{1f}) of about 18%. Therefore, the electrically injected magnons from the Pt injector reaching the Pt detector decrease by 18% by reorienting the magnetization direction of the Py gate electrode.

As the signal for magnon propagation to the Pt detector decreases at higher field B, it becomes relevant to consider the complementary signal R_{NL}^{1f} measured across the middle Py

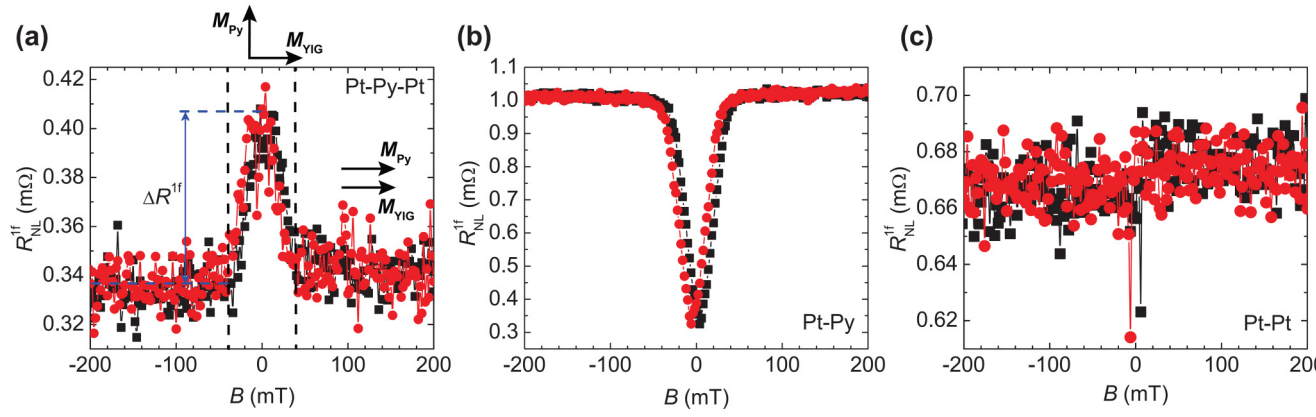

FIG. 2. Magnetic field (B) is swept by increasing the field (trace, black) and decreasing the field (retrace, red) along the x axis and the first harmonic response of the nonlocal magnon spin signal (R_{NL}^{1f}) is measured by (a) Pt as injector and detector in a device with a 900 nm wide Py middle strip (Pt-Py-Pt), (b) Pt as injector and the 900 nm wide middle Py strip as detector (Pt-Py), and (c) Pt as injector and detector in a reference device without any middle Py strip (Pt-Pt). The arrows in (a) indicate the relative orientation of the magnetizations of Py and YIG. Py has a thickness of 9 nm.

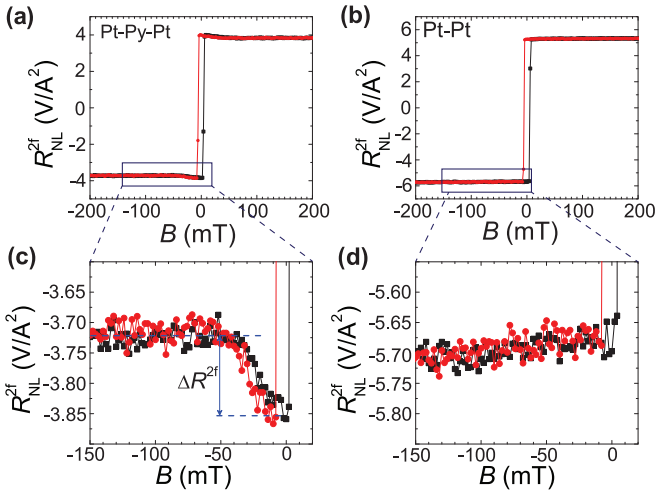

FIG. 3. Second harmonic response of the nonlocal magnon spin signal (R_{NL}^{2f}), measured as a function of B, by (a) the Pt detector in a device with a 900 nm wide Py middle strip and (b) in a reference device without a middle Py strip. Magnified regions from the graphs in (a) and (b) are shown in (c) and (d), respectively, demonstrating the effect of the middle Py strip on R_{NL}^{2f}. The data shown in black and red represent the trace and retrace directions, respectively.

strip, which is shown in Fig. 2(b). If the decrease in magnon propagation to the Pt electrode is due to magnon absorption at the Py strip, then in the latter we expect to see an opposite response: increasing magnon detection at higher field. Such a response is indeed observed. However, note that the signal modulation in the Py detector is of more than 210%. To quantitatively understand this large modulation we consider the distinct detection mechanisms at play at the Py strip. The detection of nonlocal magnon transport at the Py strip occurs via a combination of ISHE (also present in Pt) and the inverse anomalous spin Hall effect (IASHE, absent in Pt), resulting in a detection efficiency that depends on the orientation of M_{Py} and leading to a line shape consistent with previous reports [14,15]. In particular, at low field the detection efficiency of Py (measured relative to that of Pt) is dominated only by ISHE and has a value $\eta(\text{Py/Pt}) \sim 0.55$, whereas at higher B it evolves into being given by both IASHE and ISHE, reaching a value of $\eta(\text{Py/Pt}) \sim 1.1$ [see Fig. 3(d) in Ref. [15]]. The modulation of the detection efficiency in the Py strip is caused by a change in the efficiency to convert a spin accumulation into a charge current. Therefore, we expect a modulation which is one order of magnitude larger, and of a different nature, than the 18% modulation seen in Fig. 2(a) for the Pt detector.

The nonlocal signal measured in a reference Pt-Pt device, without any middle Py strip, is shown in Fig. 2(c). R_{NL}^{1f} was found to be constant in this reference device, which evidences the role of the middle Py strip in the modulation of R_{NL}^{1f} in the nonreference devices, as shown in Fig. 2(a). Therefore, we can modulate the magnon current reaching the Pt detector using the Py gate, due to a modulation of the magnon absorption in the Py.

The second harmonic response of the nonlocal magnon signal (R_{NL}^{2f}) was also measured by sweeping B along the x axis, as shown in Figs. 3(a)–3(d). The magnetic gating effect of the middle Py strip also led to a modulation in R_{NL}^{2f} measured by the Pt detector, as depicted in Figs. 3(a) and 3(c). However, the modulation in R_{NL}^{2f} was found to be $\Delta R^{2f} \approx 3.6\%$, which is five times smaller than that of R^{1f}. Note that the second harmonic response is related to the nonequilibrium magnons which are generated via the spin Seebeck effect (SSE) in YIG [4,10,16], driven by the thermal gradient created by the Pt injector due to Joule heating. The spacing between injector and detector is large and it corresponds to a magnon accumulation at the detector, confirmed by the correct sign of the second harmonic response [17]. The transmission of these thermally generated magnons into the middle Py strip also depends on the relative orientation of M_{Py} and M_{YIG}, resulting in the modulation of R_{NL}^{2f} [Figs. 3(a) and 3(c)]. To rationalize the smaller modulation in the $2f$ signal, as compared to the $1f$ signal, we have to look at the magnons generated by SSE. While the injector-detector spacing of $2\,\mu$m is large enough to ensure a magnon accumulation at the detector, this spacing is well below the magnon relaxation length (ca. $10\,\mu$m) and transport of thermally generated magnons occurs in the diffusive regime [18]. In this regime, the radial thermal gradient created by the heater extends through the YIG under the magnetic gate and, therefore, thermally generated magnons are not only generated close to the injector, but also nonlocally within the bulk region between the injector and detector [17,18]. Magnons accumulate at the bottom of the YIG film and then diffuse towards the detector [18]. Therefore, less thermally generated magnons cross the modulator at the interface while diffusing towards the detector, which results in a relatively smaller modulation of the second harmonic signal in comparison to the first harmonic signal. Note that the total magnitude of R_{NL}^{2f} is reduced compared to the case of having no middle Py strip in the reference Pt-Pt device, as shown in Figs. 3(b) and 3(d). In this reference device, there is no modulation in R_{NL}^{2f} with B.

Furthermore, we study the dependence of the modulation of the nonlocal magnon spin signals on the width of the middle Py gate (w_{Py}). We define a relative modulation for the first (ΔR^{1f}) and second harmonic (ΔR^{2f}) signals and a total modulation (ΔR^{tot}) of the spin signal, as depicted in Fig. 4(a). $\Delta R^{1f(2f)}$ gives the modulation only due to the magnetization orientation dependent magnetic gating effect, whereas ΔR^{tot} gives the total modulation of the spin signal compared to the reference device (without any middle Py strip). The modulator acts as a magnon absorber; therefore, ΔR^{tot} is finite and similar in nature as when a Pt modulator is used [9]. On top of this modulation we observe the magnetic gating effect, which is only observed when a magnetic modulator (Py) is used and is defined by the relative modulation $\Delta R^{1f(2f)}$. We find a linear dependence of $\Delta R^{1f(2f)}$ on w_{Py} for both first (second) $1f$ ($2f$) harmonic response of the spin signal, as shown in Fig. 4(b). Also, the variation in $\Delta R^{1f(2f)}$ between two different batches of devices (depicted as open and filled symbols) is very small, demonstrating the reproducibility of the magnetic gating effect. In the case of the total modulation ΔR^{tot}, although it exhibits an increasing trend with w_{Py}, the results are dominated by a batch-to-batch variability. We attribute this variability to the difference in transparencies at Pt | YIG and Py | YIG interfaces amongst the different batches of devices.

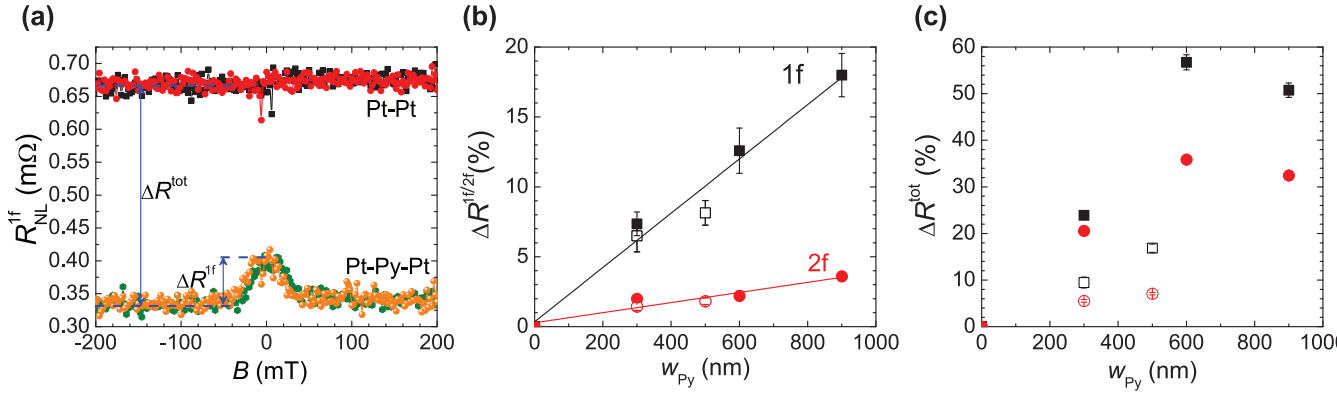

FIG. 4. (a) R_{NL}^{1f}, measured by the Pt detector in the reference device without the middle Py strip [black(trace)-red(retrace)] and in the device with a 900 nm wide middle Py strip [green(trace)-orange(retrace)] are plotted together, illustrating the relative modulation ($\Delta R^{1f(2f)}$) and the total modulation (ΔR^{tot}) in the nonlocal magnon spin signal. $\Delta R^{1f(2f)}$ (b) and (ΔR^{tot}) (c) are plotted as a function of the middle Py width (w_{Py}). The black squares and the red circles represent the modulations in the first and the second harmonic response of the nonlocal signal, respectively, while the open and the filled symbols correspond to devices from two different batches. The linear dependence of $\Delta R^{1f(2f)}$ on w_{Py} is evident from the linear fits (solid lines) to the data in (b). $\Delta R^{1f/2f}(\%)$ and $\Delta R^{tot}(\%)$ are defined as $\Delta R^{1f/2f}(\%) = \Delta R^{1f/2f}/R^{1f/2f}(|B| \geqslant 50$ mT) and $\Delta R^{tot}(\%) = \Delta R^{tot}/R^{Pt\text{-}Pt}$.

As per the definitions in the caption of Fig. 4, the normalized $\Delta R^{tot}(\%)$ depends on the total magnon absorption by the magnetic gate, relative to a different (reference) device that does not possess a magnetic gate. Therefore, ΔR^{tot} depends on the absolute signal and the reproducibility of interface quality for all interfaces. On the other hand, $\Delta R^{1f(2f)}(\%)$ is the modulation, $\Delta R^{1f(2f)}$, normalized by the signal $R^{1f(2f)}$ within the same device. The latter is sensitive only to variations in the Py | YIG interfaces, which are all simultaneously fabricated since we only change the width of the magnetic gate. Therefore, $\Delta R^{tot}(\%)$ has a larger variability, while $\Delta R^{1f(2f)}(\%)$ exhibits a clearer linear scaling with w_{Py}. Note that given the long magnon relaxation length in YIG ($\approx$10 μm) [4], the decay of the magnon chemical potential is expected to be small on the length scale of our narrow magnetic gates, with a width of only $w_{Py} \leqslant 0.9$ μm. Considering the magnon chemical potential to be approximately constant on this narrow scale leads to a magnon absorption proportional to the area of the magnetic gate. Therefore, the linear scaling with w_{Py} further supports the magnetization orientation dependent magnon absorption into the middle Py gate.

Finally, we study the dependence of the modulation of the nonlocal magnon spin signals on the thickness (t_{Py}) of the middle Py strip. $\Delta R^{1f(2f)}$ and ΔR^{tot} as a function of Py thickness is shown in Figs. 5(a) and 5(b). $\Delta R^{1f(2f)}$ and ΔR^{tot} show an increase for increasing Py thickness up to 15 nm, after which $\Delta R^{1f(2f)}$ and ΔR^{tot} show a decrease for increasing Py thickness. Note that, for this batch of devices, we first fabricated the Pt electrodes for all devices simultaneously within the same substrate, followed by sequential fabrication of the magnetic gates for each desired thickness. Therefore, this batch of devices with different Py thicknesses involves a difference of at least one additional lithography step between devices with different Py thicknesses. This can significantly influence the Py | YIG and Pt | YIG interface, causing the difference in ΔR^{tot} and $\Delta R^{1f(2f)}$ between the first two and the third batch of devices. Besides, the Gilbert damping in Py is lower for thicker Py films [19], meaning a longer magnon relaxation length and therefore the finite probability of magnons traveling into the Py and back into the YIG is larger for thicker Py films than for thinner Py films. This can explain the lower $\Delta R^{1f(2f)}$ modulation using a thicker Py gate.

IV. SUMMARY AND OUTLOOK

In this study, we have demonstrated efficient modulation of nonlocal magnon spin transport in a magnetic insulator using a magnetic gate in a proof-of-concept transistor device geometry. We achieve a modulation of up to an order of magnitude larger than a previously reported three-terminal magnon transistor [9] with the same YIG thickness, where the spin transport was modulated by creating a nonequilibrium magnon density in the YIG channel via an electrically driven Pt gate. In this work we show that the spin transport in the YIG channel is modulated in (or close to) equilibrium at the ferromagnetic metal | magnetic insulator interface, where the magnon transmission at the interface is controlled by manipulating the magnetization direction of a magnetic gate. A decrease in the magnon current is observed for parallel orientation of the

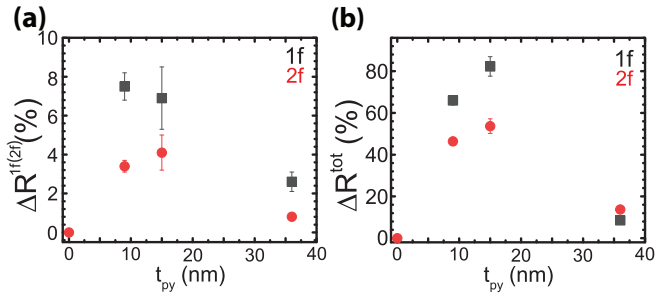

FIG. 5. $\Delta R^{1f(2f)}$ (a) and ΔR^{tot} (b) are plotted as a function of the thickness of the middle Py strip (t_{Py}), which has a width of 900 nm. The black squares and the red circles represent the modulations in the first and the second harmonic response of the nonlocal signal, respectively.

magnetizations. Therefore, we conclude that spin-flip scattering and magnon to magnon transmission dominates over spin transfer torque at ferromagnetic metal | magnetic insulator interface. The origin of the magnetic gating effect is either an enhancement of spin-flip scattering or magnon to magnon transmission at the Py | YIG interface. We propose that such a magnetic gate can be used for future magnon transistor spin logic applications and memory applications embedded in the ferromagnetic gate, which can be used in programmable magnonics devices.

ACKNOWLEDGMENTS

We acknowledge the technical support from J. G. Holstein, H. M. de Roosz, H. Adema T. Schouten, and H. de Vries. We acknowledge the financial support of the Zernike Institute for Advanced Materials and the Future and Emerging Technologies (FET) programme within the Seventh Framework Programme for Research of the European Commission, under FET-Open Grant No. 618083 (CNTQC). This project is also financed by the NWO Spinoza prize (2016) awarded to B.J.v.W. by the NWO.

[1] A. V. Chumak, V. I. Vasyuchka, A. A. Serga, and B. Hillebrands, Nat. Phys. **11**, 453 (2015).
[2] T. Jungwirth, X. Marti, P. Wadley, and J. Wunderlich, Nat. Nanotechnol. **11**, 231 (2016).
[3] V. Baltz, A. Manchon, M. Tsoi, T. Moriyama, T. Ono, and Y. Tserkovnyak, Rev. Mod. Phys. **90**, 015005 (2018).
[4] L. J. Cornelissen, J. Liu, R. A. Duine, J. B. Youssef, and B. J. van Wees, Nat. Phys. **11**, 1022 (2015).
[5] A. V. Chumak, A. A. Serga, and B. Hillebrands, Nat. Commun. **5**, 4700 (2014).
[6] H. Wu, L. Huang, C. Fang, B. S. Yang, C. H. Wan, G. Q. Yu, J. F. Feng, H. X. Wei, and X. F. Han, Phys. Rev. Lett. **120**, 097205 (2018).
[7] C. Y. Guo, C. H. Wan, X. Wang, C. Fang, P. Tang, W. J. Kong, M. K. Zhao, L. N. Jiang, B. S. Tao, G. Q. Yu, and X. F. Han, Phys. Rev. B **98**, 134426 (2018).
[8] J. Cramer, F. Fuhrmann, U. Ritzmann, V. Gall, T. Niizeki, R. Ramos, Z. Qiu, D. Hou, T. Kikkawa, J. Sinova *et al.*, Nat. Commun. **9**, 1089 (2018).
[9] L. J. Cornelissen, J. Liu, B. J. van Wees, and R. A. Duine, Phys. Rev. Lett. **120**, 097702 (2018).
[10] L. J. Cornelissen, K. J. H. Peters, G. E. W. Bauer, R. A. Duine, and B. J. van Wees, Phys. Rev. B **94**, 014412 (2016).
[11] S. R. Boona and J. P. Heremans, Phys. Rev. B **90**, 064421 (2014).
[12] E. Chavez-Angel, R. A. Zarate, S. Fuentes, E. J. Guo, M. Kläui, and G. Jakob, New J. Phys. **19**, 013011 (2017).
[13] N. Vlietstra, J. Shan, V. Castel, B. J. van Wees, and J. Ben Youssef, Phys. Rev. B **87**, 184421 (2013).
[14] K. S. Das, J. Liu, B. J. van Wees, and I. J. Vera-Marun, Nano Lett. **18**, 5633 (2018).
[15] K. S. Das, W. Y. Schoemaker, B. J. van Wees, and I. J. Vera-Marun, Phys. Rev. B **96**, 220408(R) (2017).
[16] K. Uchida, J. Xiao, H. Adachi, J. Ohe, S. Takahashi, J. Ieda, T. Ota, Y. Kajiwara, H. Umezawa, H. Kawai, G. E. W. Bauer, S. Maekawa, and E. Saitoh, Nat. Mater. **9**, 894 (2010).
[17] J. Shan, L. J. Cornelissen, N. Vlietstra, J. Ben Youssef, T. Kuschel, R. A. Duine, and B. J. van Wees, Phys. Rev. B **94**, 174437 (2016).
[18] J. Shan, L. J. Cornelissen, J. Liu, J. B. Youssef, L. Liang, and B. J. van Wees, Phys. Rev. B **96**, 184427 (2017).
[19] Y. Zhao, Q. Song, S.-H. Yang, T. Su, W. Yuan, S. S. Parkin, J. Shi, and W. Han, Sci. Rep. **6**, 22890 (2016).